Proceedings of BALTTRIB'2022 edited by prof. J. Padgurskas
eISSN 2424-5089 (Online)
DOI: 10.15544/balttrib.2022.6

NUMERICAL MODELING OF SINGLE-ASPERITY FRICTIONAL CONTACT WITH ADHESION

A. Palaiologos, P.G. Nikolakopoulos*
Department of Mechanical Engineering and Aeronautics, University of Patras, Greece

Abstract. In our research, the elastic contact between a sphere and a flat surface is investigated, under the combination of normal and tangential loads, with the simultaneous presence of friction and adhesion. Based on the Boussinesq-Cerruti integral equations, a numerical model was created to calculate the surface tractions and displacements. Maximum shear tractions on the contact interface, and therefore friction, are governed by a bond/material failure mechanism instead of the typical Coulomb friction law. Adding to the generality of our model, a local traction-separation law was enforced for the simulation of normal and shear tractions attributed to the adhesion of the contacting bodies, therefore enabling the interaction between friction and adhesion. Our research aims to extract all the necessary mathematical formulas to describe the response of a spherical tip asperity in contact with a flat surface under normal and tangential loads in the presence of friction and adhesion.

Keywords. contact mechanics, static friction, adhesion, asperity contact, traction separation law.

1. INTRODUCTION

Bibliography is filled with a vast number of analytical and numerical models for the simulation of single asperity contacts. The first continuum mechanics contact model dates back to 1881 and the pioneering work of Hertz [1]. In his work, Hertz studied the frictionless normal contact between two elastic spheres and produced the first analytical solutions regarding the contact area and pressure. However, his assumption of frictionless contact is invalid in the case where the two contacting bodies are dissimilar and/or under the presence of tangential loads. Under the presence of tangential loads, the shear tractions on the contact area can locally surpass the static friction limit. Therefore, the phenomenon called microslip can occur, where in parts of the contact area the two body surfaces are slipping to each other, whereas in the rest of the contact area the two body surfaces are sticked together. Under increasing tangential loads, the slip areas increase while the stick areas decrease, leading to the gross sliding of the contact. Cattaneo [2] and Mindlin [3], in the first half of the 20th century, came up with the exact solution for the partial slip of cylindrical frictional contacts, which can also be validly extended to circular contacts. However, their solutions came under the assumption of similar materials and fail to depict the coupling between shear and normal tractions.

Over the years there have been numerous attempts for the numerical simulation of a dry frictional contact, either by utilizing the finite element and the boundary element methods or by semi analytical ones. The one that we distinguished during our research is the work from Chen and Wang [4], who created a semi analytical model, based on the Boussinesq-Cerruti integral equations for normal and tangential point contact, that utilizes the conjugate gradient technique (CGM) by Polonski and Keer [5], as well as the discrete convolution Fast Fourier Transform (DC-FFT) algorithm by Liu et al. [6], to model the contact of dissimilar materials under combined normal and tangential loads. Their model is able to depict the incipient of sliding of the contact under the effect of the tangential loads while taking into account the coupling between shear and normal tractions. However, the shear traction limit was defined by a localized coulomb friction law, which although convenient, was problematic. The reasons

* Author for contacts: Prof. Pantelis Nikolakopoulos
E–mail: pnikolak@mech.upatras.gr

are the a priori estimation of friction coefficient, which for the case of asperity contact is impossible, and the possibility of calculating high shear tractions that exceeded the shear strength of material.

This drawback was addressed by a subsequent paper [7] where the upper shear traction limit was determined by the material properties of the bodies, by replacing the localized Coulomb friction law with the Tabor's equation. Shi [8] in his work regarding the slip incipient in dry smooth frictional contacts theorized that the slip incipient is either due to the interfacial bond failure under low normal loads, or due to soft material failure under high normal loads. In the case of high normal loads, the contact is plastic, and the Von Mises criterion of the softer material should dictate the onset of slip. In the case of low normal loads, the contact is elastic, and an alternate criterion (which he left undefined) should be used. Tabor contributed greatly to our understanding of the friction mechanisms, including adhesion and ploughing. He introduced the concept of junction growth and pointed out three main factors involved in the friction of dry contacts [9], namely: the true contact area, the nature and strength of junctions formed at the interface, and the way which materials are sheared and raptured. In a previous paper regarding the junction growth in metallic frictional contacts [10], he came up with his famous equation relating the local shear and normal strength of the contact to the hardness of the softer material. Furthermore, he concluded that in ambient environment the strength of the contact should be lower than in bulk due to the presence of oxides and contaminants on the surfaces of the contacting bodies.

As stated in [11], adhesion is generally not negligible at small scales, which is proven by experimental results at sub-micro/nano scale. Therefore, since our research focuses on the elastic contact of asperities it was deemed crucial for the generality of our model to consider the effect of adhesion on the contact. There exist several continuum mechanics models for adhesive contacts that utilize the Hertzian approach. The first adhesive contact models were proposed in the 1930s by Bradley [12], who considered the full interaction potential between two rigid spheres, and Derjaguin [13], who included only the attractive part end assumed a steep repulsive part for the potential that prohibited the interpenetration of the two spheres. Derjaguin also considered the deformation of the spheres. Almost 40 years later, Derjaquin together with Muller and Toporov [14] proposed the famous DMT adhesive contact theory, by assuming Hertzian contact between the deformable bodies and additional adhesive interaction forces acting around the contact area, that didn't change the shape of the contacting bodies. In 1971 Johnson, Kendall and Roberts came up with the JKR adhesion model [15], where the Hertzian contact pressure is offset by short range attractive surface stresses acting only within the contact area. The DMT and JKR theories were thought at first to be contradictory, but it was proven later by Tabor [16] that these theories could be considered as the opposite extremes for adhesive contact of deformable bodies. The DMT theory is more suitable for the contact of small and stiffer bodies whereas the JKR theory describes better the adhesion between large and compliant bodies. To quantify these limits of adhesion and the cases in between, the famous Tabor's parameter was defined, which is equal to the ratio of elastic surface displacement at the moment of separation to the effective range of adhesion forces. JKR applies to large values whereas DMT applies to small values of Tabor's parameter. Many researchers have created models to bridge the gap between DMT and JKR theories [17–20], with the most widely used being the Maugis-Dugdale model [21]. Furthermore, to aid in the selection of the most suitable adhesive contact model special maps have been proposed [22,23] depicting the suitability of the most famous adhesive theories for different cases of load and Tabor's parameter values.

Despite being well established and widely used, the aforementioned models consider the adhesion's effect on the contact only on the normal direction. On the same time, they neglect the existence of microslip and tangential tractions in the contact zone. That rises the question: how does adhesion affect interfacial shear stress and vice versa? The first one said that question where Savkoor and Briggs [24] who investigated a JKR-type adhesive contact under no slip assumption and infinite shear stress near the edges of the contact. They concluded that under the same normal load the pull force and contact radius became smaller. Mc Meeking et al. [25] and Peng et al. [26] also studied the impact of frictional shear stress on adhesive JKR and M-D contact respectively with partial and gross slip. Their energy analyses included, however, many limiting assumptions like uniform shear stress along the contact, incompressible bodies, as well as complex mathematical formulas. Another approach to simulate the adhesive contact under combined loads is the use of traction separation laws. This approach has been used widely in fracture mechanics where the mathematical expressions describing the problem draw

similarities with the ones used in contact mechanics. Rafols et al [27] investigated the sliding incipient under both friction and adhesion for 2D contacts (cylinder on plane) by using a modified cohesive zone model for the adhesive part of the tractions, created by McGarry et al. [28]. The elastic part of the fractions was calculated using Green's functions like in Chen et al. [4].

2. THEORETICAL MODEL

Our research goal is the creation of a semi analytical model of an asperity-level contact, under the presence of both friction and adhesion. Although our model bears some resemblance to the ones made by Chen et al. [4,7] and Bazrafshan et al. [29], it manages to include adhesion in normal and tangential directions, while simultaneously utilising a partial slip criterion based on the material properties of the contacting bodies rather than in an a priori estimation of an arbitrary friction coefficient. For the sake of brevity, we will avoid the extensive description of the model and instead just mention the alterations made, whilst referring to the bibliography for the algorithms our model was based on.

The main core of our model comes from the work of Chen et al. [4,7]. By utilising the DC-FFT/CGM algorithm in [4] we are able to simulate the microslip phenomenon due to material dissimilarity during normal and tangential loading. The algorithm is modified slightly to turn from load-driven into displacement-driven. In this way the rigid body movements on the normal (δ_z) and lateral (δ_x, δ_y) directions become input parameters, instead of being estimated, and the contact loads (F_x, F_y, F_z) are calculated by the model. At this point we should mention that the correction step for the δ_x and δ_y at the end of the iteration (eq. 23 in [4]) is excluded in our model.

Our next step is to replace the Chen and Wang' friction criterion [7] with Shi's slip incipient mechanism [8]. For the coupling between the maximum allowed normal (p_{max}) and shear (q_{max}) tractions we incorporated the Tabor equation [10] for contaminated surfaces for the case of low normal loads (bond failure) and the Von Mises criterion for the case of high loads (material failure). According to Tabor [10] in ambient environment the shear strength of the surface should be lower than in bulk due to the presence of oxides and contaminants on the surfaces of the contacting bodies. Under low loads the layer of oxides/contaminants is not broken, and the contact's shear strength is dictated by the surface shear strength. Tabor's equation for that case is:

$$p^2 + \frac{q^2}{k_{VM}{}^2} = \frac{T_S{}^2}{k_{VM}{}^2} \tag{1}$$

Where T_S is the bulk shear strength, and $k_{VM}=T_S/S_Y\approx\sqrt{3}$ is the shear to yield strength ratio of the softer material. By setting $T_S=T_{Si}/k_\tau$ and $q=T_{Si}$, with T_{Si} being the surface's shear strength, one gets:

$$\frac{q}{p} = k_{VM}\Big/\sqrt{k_T{}^{-2}-1} \tag{2}$$

Under high loads the layer of oxides/contaminants is fully broken the coupling p_{max} and q_{max} is determined by material failure mechanisms, and for our case by the von Mises criterion:

$$p^2 + \frac{q^2}{k_{VM}{}^2} = S_Y{}^2 \tag{3}$$

The shear tractions at the contact interface must be less or equal to the smaller q_{max} given by eqs. (2) and (3), and the stick and slip areas are determined accordingly, as in [7].

To account for the effect of the adhesion on the contact, a traction-separation law proposed by McGarry et al. [28] is used to add an adhesive component on both normal and shear tractions. We selected the "separation magnitude coupling" law (SMC), in which the adhesive normal (p_{adh}) and shear (q_{adh}) tractions are:

$$\begin{aligned} p_{adh} &= -\sigma_{max}(h/\delta_n)exp\left(1-\sqrt{(h/\delta_n)^2+(s/\delta_t)^2}\right) \\ q_{adh} &= -\tau_{max}(s/\delta_t)exp\left(1-\sqrt{(h/\delta_n)^2+(s/\delta_t)^2}\right) \end{aligned} \tag{4}$$

Where σ_{max} and τ_{max} are the maximum and normal tractions, whereas δ_n and δ_t are the normal and tangential characteristic lengths respectively. h is the gap between the surfaces of the two bodies in the

normal direction of the contact, and s is the tangential slip between the two surfaces. In our model, normal and shear tractions comprise of an elastic and an adhesive component. The elastic tractions undergo the altered displacement-driven DC-FFT/CGM algorithm as mentioned above, whereas the adhesive part of the tractions is calculated as in eq. (4) from the updated normal gap and tangential slip at the end of each iteration of the CGM algorithm. The two components are then added to give the total normal and shear tractions for the contact, and the process is repeated until convergence in the same way as in [4, 7]. Similar to [29], we divide the total contact area to an elastic contact part and an adhesive contact part. On the first part the elastic and adhesive tractions apply and on the second part only the adhesive portion of tractions applies. On both parts of the total contact area the normal gap between the surfaces of the two bodies is zero.

3. RESULTS AND DISCUSSIONS

Our model is used to simulate the adhesive frictional contact of a copper spherical-tipped asperity, with a radius R=10 μm, on a hardened steel flat surface. The mechanical properties of the two bodies are given in Table 1. For the simulation, four different contact depths (δ_z) and three surface-to-bulk strength ratio (k_τ) values were selected. To study the effect of adhesion, the tests were conducted with and without the adhesive components of the normal and shear tractions. Under these conditions, the friction coefficient of the contact as well as the microslip phenomenon were investigated.

Table 1. Mechanical Properties of contacting bodies.

Properties (Units)	**Copper asperity**	**Hardened Steel flat surface**
Young's Modulus (GPa)	106	205
Poisson Ratio (–)	0.33	0.31
Hardness (GPa)	1.0	6.2
Yield Strength (MPa)	200	345

In Table 2 the maximum lateral rigid body movement (δ_x) before gross slip for the asperity and the respective static friction coefficient (μ) are shown, for different values of contact depths and surface-to-bulk strength ratios.

Table 2. Maximum lateral body movement (δ_x) before gross slip and static friction coefficient (μ) for variable contact depths (δ_z) and surface-to-bulk strength ratios (k_τ).

	kτ=0.50				**kτ=0.80**				**kτ=0.95**			
Contact	**Adhesionless**		**Adhesive**		**Adhesionless**		**Adhesive**		**Adhesionless**		**Adhesive**	
δz (μm)	δx (μm)	μ	δx (μm)	μ	δx (μm)	μ	δx (μm)	μ	δx (μm)	μ	δx (μm)	μ
1.0e–5	4.2e–6	0.332	4.4e–6	0.340	9.6e–6	0.769	1.0e–5	0.788	2.2e–5	1.755	2.3e–5	1.798
5.0e–5	2.1e–5	0.332	2.4e–5	0.350	4.8e–5	0.769	5.4e–5	0.809	6.7e–5	1.250	7.5e–5	1.277
1.0e–4	4.2e–5	0.332	4.9e–5	0.357	7.3e–5	0.665	8.5e–5	0.688	8.2e–5	0.827	9.5e–5	0.843
1.5e–4	5.5e–5	0.308	6.5e–5	0.325	7.7e–5	0.495	8.8e–5	0.502	8.5e–5	0.583	9.8e–5	0.587

The first thing that must be noted is that the presence of adhesion increases noticeably the maximum lateral rigid body movement at which gross slip occurs. That increase is more prominent at larger contact depths and smaller surface-to-bulk strength ratios, possibly due to the adhesive traction components being on the same scale with the elastic ones. Static friction coefficient is also slightly increased. It is also observed that surface-to-bulk strength ratio significantly affects the values and the behaviour of the static friction coefficient and the maximum lateral rigid body movement. This is due to k_τ dictating the influence of each partial slip mechanism. At low values of k_τ the shear strength of the surface is significantly lower than the bulk value and the contact is governed by the low shear strength of the oxidized/contaminated surface, whereas at high kt values the surface shear strength approaches the bulk shear strength value, which results in the shear strength of contact being determined by the material strength. Therefore, we see that for k_τ=0.50, static friction coefficient obtains a small, fixed value, determined by the surface shear strength. Only for the largest contact depth the static friction coefficient is reduced because the normal pressures are big enough to fully break the contaminated/oxidised layer

on the surface and cause localized yielding of the material in the contact area. For the case of k_τ=0.80 the same phenomenon takes place, albeit at smaller values of δ_z. Here interfacial bond failure and material failure affect equally the strength of the contact. As a result, at small contact depths (low normal pressures) static friction coefficient is determined by the interfacial bond shear strength and acquires a fixed value, whereas at larger contact depths (high normal pressures) start friction coefficient comes from the bulk shear strength and decreases as the contact depth increases. Finally, for the case of k_τ=0.95 contact shear strength is almost exclusively determined by the material shear strength since the static friction coefficient decreases monotonically with increasing contact depths. We should also mention that k_τ also describes the interfacial bond strength, and as a result we see that increasing k_τ results in larger static friction coefficient values. Under the presence of adhesion, the trend of the static friction coefficient is altered. Instead of acquiring a fixed value, at smaller contact depths, for the cases where interfacial bond strength affects the contact strength (k_τ=0.50 and k_τ=0.80), the static friction coefficient is increasing together with the contact depth. At larger δ_z values the static friction coefficient decreases significantly. However, for the case of k_τ=0.95, where contact strength depends almost exclusively on the material shear strength, the static friction coefficient decreases monotonically like the adhesionless contact.

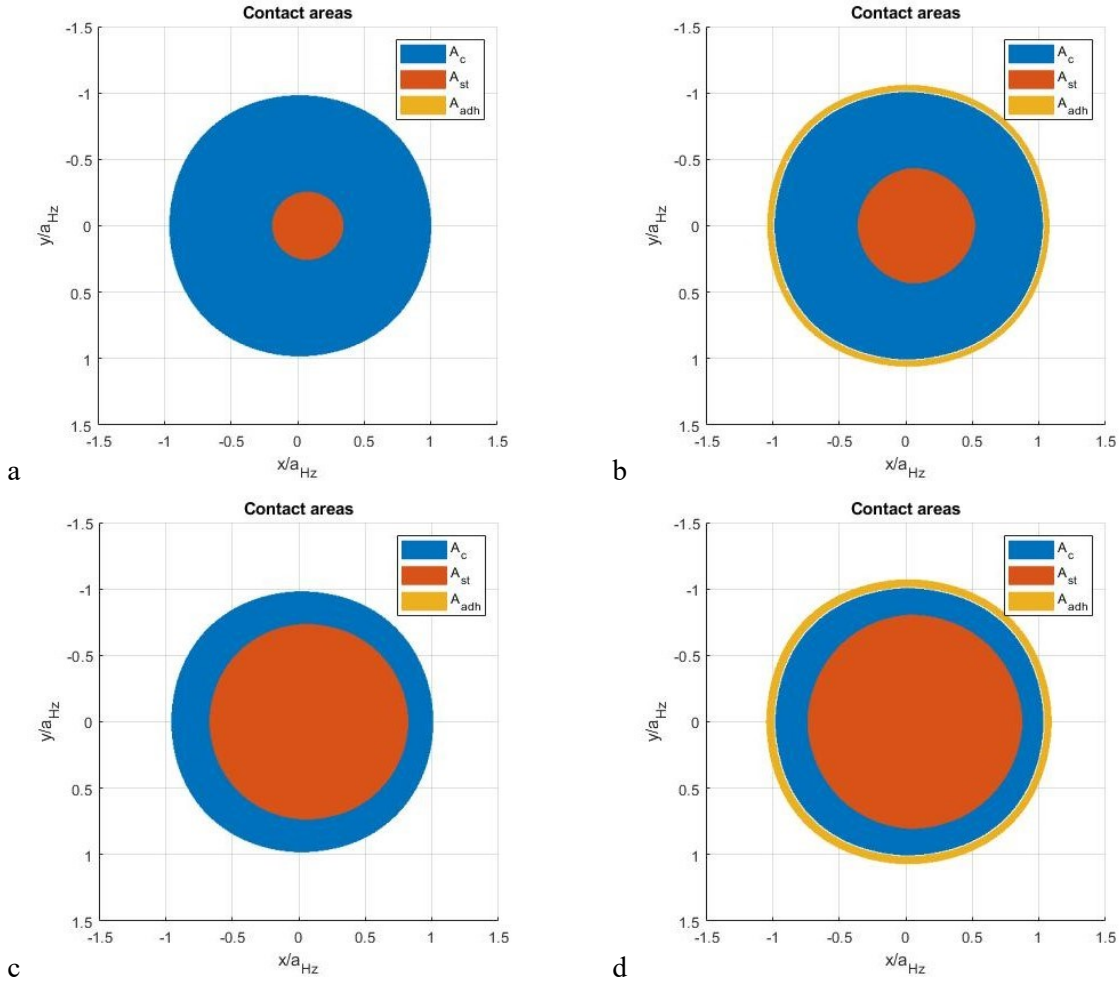

Figure 1. Elastic contact (A_c), stick (A_{st}) and adhesive contact (A_{adh}) areas during the partial slip phenomenon for contact depth δ_z=5.0e–5 μm and lateral rigid body movement δ_x=4.5e–5 μm, for a) kτ=0.80 without adhesion, b) kτ=0.80 with adhesion, c) kτ=0.95 without adhesion, d) kτ=0.95 with adhesion.

In Figure 1 the microslip phenomenon is depicted for small contact depths (δ_z=5.0e–5 μm) and lateral rigid body movement δ_x=4.5e–5 μm, for two surface-to-bulk strength ratios (k_τ=0.80 for Figures 1a and 1b and k_τ=0.95 for Figures 1c and 1d) under the presence of adhesion (Figures 1a and 1c) and without it (Figures 1b and 1d). The "elastic" contact area (A_c) is depicted in blue, the stick area (A_{st}) in orange and the "adhesive" contact area (A_{adh}) in yellow. The total contact area is comprised of the areas Ac

(where the elastic and adhesive tractions apply) and A_{adh} (where only the adhesive portion of tractions applies). The first general observation is that the presence of adhesion enlarges not only the total contact area, but also the stick area. The attractive adhesive tractions bring the surfaces of the bodies closer, creating a rim of solely adhesive contact area, thus contributing to the increase of the total contact area and the junction growth. The increased contact area can now sustain higher normal and shear loads because the adhesive component reduces the total normal contact pressure all over the area. This means that if the maximum shear stresses (determined by eqs. 2 and 3) that can be applied at the contact interface is higher, and as a result a larger portion of the contact area will be in stick. Furthermore, the lateral adhesive tractions contribute slightly to a sticking between the two bodies. The next observation that can be made has to do with the stick area. For both cases of k_τ values it is evident that the stick area increases together with the surface-to-bulk shear strength ratio. This is because higher k_τ means higher interfacial bond strength, thus a more material-failure dependent contact. Therefore, at k_τ=0.95 (Figures 1c and 1d) the more prominent material failure mechanism allows for higher shear stresses on the contact interface, thus enabling a larger stick area. On the other hand, at k_τ=0.80 (Figures 1a and 1b) both interfacial bond and material failure mechanisms are more or less equally dominant, which means that some parts of the contact area (low normal pressure) obey the interfacial bond mechanism, whereas the rest of the contact area (high normal pressure) obey the material failure mechanism. As a result, the stick area in that case is much smaller.

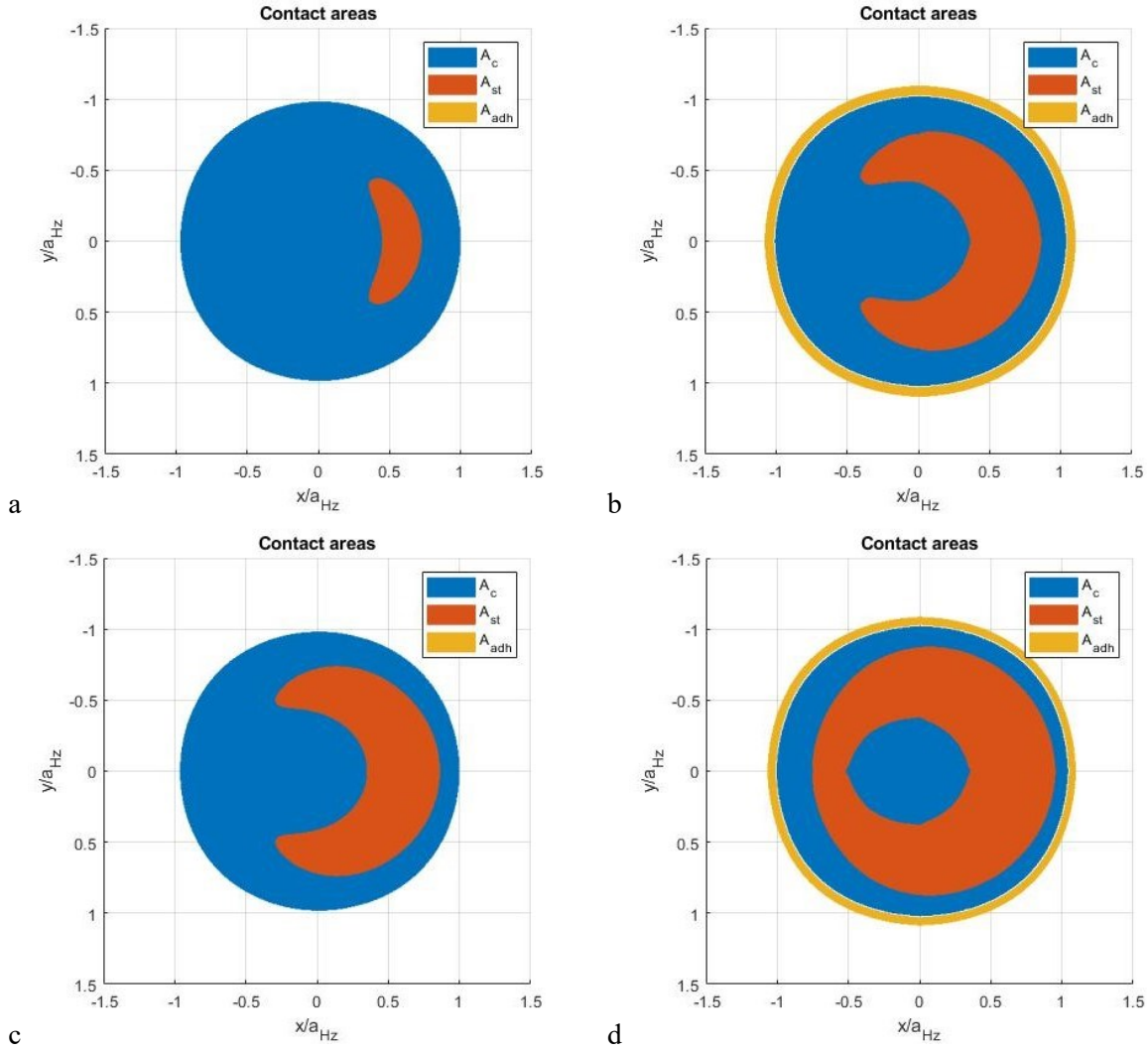

Figure 2. Elastic contact (A_c), stick (A_{st}) and adhesive contact (A_{adh}) areas during the partial slip phenomenon for contact depth δ_z=1.5e–4 μm and lateral rigid body movement δ_x=7.5e–5 μm, for a) kτ=0.80 without adhesion, b) kτ=0.80 with adhesion, c) kτ=0.95 without adhesion, d) kτ=0.95 with adhesion.

The observations made above hold also for the cases depicted in Figure 2. Here the microslip phenomenon for high contact depths (δ_z=1.5e–4 μm) and lateral rigid body movement δ_x=7.5e–5 μm for two surface-to-bulk strength ratios (k_τ=0.80 for Figures 2a and 2b and k_τ=0.95 for Figures 2c and 2d) under the presence of adhesion (Figures 2a and 2c) and without it (Figures 2b and 2d) is shown. A remark can be made for the position and the shape of the stick area (A_{st}), as the contact approaches cross slip. In all Figure 2 cases we can see that the stick area has moved towards the direction of the sliding and has transformed from a circular area to a crescent-like one (Figures 2a, 2b and 2c), or a hollow non-symmetrical disc for the case of Figure 2d. The movement of the stick area during the partial slip of the contact is a result of the material dissimilarity between asperity and flat surface and has already been observed in [4]. The main reason for the oddly shaped stick areas shown in Figure 2 is the sliding incipient mechanism that was adopted in our model. For both cases of k_τ the partial slip of the contact is determined significantly by the material failure mechanism. Due to the higher normal pressures at the centre of the contact the maximum shear stresses that can be allowed on the interface are lower than the rest of the contact area. This means that at the centre the contact area is already slipping, and the size of the stick area depends on the values of k_τ and the presence of adhesion. The higher the k_τ value, the bigger the stick area, while on the same time the presence of adhesion means larger stick area.

5. CONCLUSIONS

All in all, our model manages to simulate the adhesive frictional asperity contact between two dissimilar materials. Although our results are qualitative so far, the effect of adhesion, as well as the influence of the two slip incipient mechanisms on the contact are evident. The presence of adhesion enhances the stick of the contact and so does the prevalence of the material failure against the interfacial bond mechanism. The partial sleep phenomenal can be modelled for different stages of the contact from pure normal contact, up to the point of gross slip. The surface-to-bulk shear strength ratio (k_τ) is the parameter that determines the influence for each of the two slip incipient mechanisms on the partial slip phenomenon during the contact. Lower values of k_τ mean lower shear strength for the oxidised surface layer compared to the bulk shear strength of the material, and on the same time prevalence of the interfacial bond failure mechanism over the material failure mechanism. For higher k_τ values, the material failure mechanism is more prominent. Due to the size and the nature of the contact (slip incipient), the most suitable experimental method to fine tune and eventually validate our model would be the Atomic Force Microscopy (AFM). Experiments are considered as the next major step of our research to determine the exact value of k_τ for a variety of contact cases regarding the materials selected, the environment where contact takes place in and many other contributing factors.

REFERENCES

[1] Hertz H. On the contact of elastic solids. Z. Reine Angew. Mathematik, 92 (1881), 156–171.
[2] Cattaneo C. Sul contatto de due corpi elastici: Distribuzione locale deglisforzi. Rendiconti dell'Accademia nazionale dei Lincei, 27 (1938), 342–348.
[3] Mindlin R.D. Compliance of Elastic Bodies in Contact. Journal of Applied Mechanics, 16(3) (1949), 259–268.
[4] Chen W.W., Wang Q.J. A numerical model for the point contact of dissimilar materials considering tangential tractions. Mechanics of Materials, 40(11) (2008), 936–948.
[5] Polonsky I.A., Keer L.M. A numerical method for solving rough contact problems based on the multi-level multi-summation and conjugate gradient techniques. Wear, 231(2) (1999), 206–219.
[6] Liu S., Wang Q., Liu G.A versatile method of discrete convolution and FFT (DC-FFT) for contact analyses. Wear, 243(1–2), (2000), 101–111.
[7] Chen W.W., Wang Q.J. A numerical static friction model for spherical contacts of rough surfaces, influence of load, material, and roughness. Journal of Tribology, 131(2) (2009), 1–8.
[8] Shi X. On slip inception and static friction for smooth dry contact. Journal of Applied Mechanics, 81(12) (2014), 121005.
[9] Tabor D. Friction-The Present State of Our Understanding. Trans. ASME, J. Lubrication Technology, 103 (1981), 169–179.
[10] Tabor D. Junction Growth in Metallic Friction the Role of Combined Stresses and Surface Contamination. Proc. Roy. Soc. London, A, 251 (1958) 378.
[11] Shi X., Zhao Y.P. Comparison of various adhesion contact theories and the influence of dimensionless load parameter. Journal of Adhesion Science and Technology, 18(1) (2004), 55–68.

[12] Bradley R. The cohesive force between solid surfaces and the surface energy of solids. Phil. Mag. 13, (1932) 853–862.
[13] Derjaguin B. Untersuchungen über die Reibung und Adhäsion, IV. Kolloid-Zeitschrift, 69(2) (1934), 155–164. (in german)
[14] Derjaguin B.V., Muller V.M., Toporov Y.P. Effect of contact deformations on the adhesion of particles. Journal of Colloid and interface science, 53(2) (1975), 314–326.
[15] Johnson K.L., Kendall K., Roberts A. Surface energy and the contact of elastic solids. Proceedings of the royal society of London. A. mathematical and physical sciences, 324 (1558) (1971), 301–313.
[16] Tabor D. Surface Force and Surface Interactions. J. Colloid Interface Sci., 58 (1977), 2.
[17] Muller V.M., Yushchenko V.S., Derjaguin B.V. On the influence of molecular forces on the deformation of an elastic sphere and its sticking to a rigid plane. Journal of Colloid and Interface Science, 77(1) (1980), 91–101.
[18] Greenwood J. Adhesion of elastic spheres. Proc. R. Soc. Lond., A, 453 (1997), 1277–1297.
[19] Carpick R.W., Ogletree D.F., Salmeron M. A general equation for fitting contact area and friction vs load measurements. Journal of colloid and interface science, 211(2), (1999), 395–400.
[20] Schwarz U.D. A generalized analytical model for the elastic deformation of an adhesive contact between a sphere and a flat surface. Journal of Colloid and Interface Science, 261(1) (2003), 99–106.
[21] Maugis D. Adhesion of spheres: the JKR-DMT transition using a Dugdale model. Journal of colloid and interface science, 150(1) (1992), 243–269.
[22] Johnson K.L., Greenwood J.A. An adhesion map for the contact of elastic spheres. Journal of colloid and interface science, 192(2) (1997), 326–333.
[23] Yao H., Ciavarella M., Gao H. Adhesion maps of spheres corrected for strength limit. Journal of colloid and interface science, 315(2) (2007), 786–790.
[24] Savkoor A.R., Briggs G. The effect of tangential force on the contact of elastic solids in adhesion. Proceedings of the Royal Society of London. A. Mathematical and Physical Sciences, 356(1684) (1977), 103–114.
[25] McMeeking R.M., Ciavarella M., Cricrì G., Kim K.S. The interaction of frictional slip and adhesion for a stiff sphere on a compliant substrate. Journal of Applied Mechanics, 87(3) (2020), 031016.
[26] Peng B., Li Q., Feng X.Q., Gao H. Effect of shear stress on adhesive contact with a generalized Maugis-Dugdale cohesive zone model. Journal of the Mechanics and Physics of Solids, 148 (2021), 104275.
[27] Pérez-Ràfols F., Nicola L. Incipient sliding of adhesive contacts. Friction, 10(6) (2022), 963–976.
[28] McGarry J.P., Máirtín É.Ó., Parry G., Beltz G.E. Potential-based and non-potential-based cohesive zone formulations under mixed-mode separation and over-closure. Part I: Theoretical analysis. Journal of the Mechanics and Physics of Solids, 63 (2014), 336–362.
[29] Bazrafshan M., de Rooij M. B., Schipper D.J. On the role of adhesion and roughness in stick-slip transition at the contact of two bodies: A numerical study. Tribology international, 121 (2018), 381–388.